Bus Protection in Systems with Inverter Interfaced Renewables using Composite Sequence Currents

Soumitri Jena[a,1], Subhadeep Paladhi[a], Ashok Kumar Pradhan[a]

[a]*Department of Electrical Engineering, Indian Institute of Technology Kharagpur, , 721302, West Bengal, India*

Abstract

Power systems are experiencing noticeable changes in operation with the integration of a large number renewable sources, which are generally connected to the grid through inverters. With significant modulation in voltage and current during fault by the embedded controllers in the inverters, available grid protection schemes are vulnerable. The theoretical analysis and simulated case studies reveal the influencing factors on the malfunction of the conventional busbar differential protection while connected to an inverter based resource. This paper proposes a differential protection method for the busbar, connecting inverter based resources to the grid, based on composite sequence currents. The performance of the proposed method is immune to the variations due to control action in the inverter based resource and change in grid codes. The IEEE 9-bus system interconnecting a PV plant is used is used to evaluate the proposed method where the comparative assessment reveals its superiority.

Keywords: Bus protection, PV plant, differential protection, Sequence components, inverter based resources.

1. Introduction

Today power grids are incorporating more renewable plants to address the environmental concern and to exploit economic benefits [1]. In order to ensure system security, stability, and tap optimum energy, different control strategies are employed in such inverter based resources (IBRs) [2, 3, 4]. The output current from an inverter is limited during fault to avoid possible damage to it. To provide reactive power support during fault and for quick voltage restoration following it, fault ride through (FRT) principle is applied in such a plant in accordance with the grid code [5, 6, 7]. The response of such plants during fault is much different compared to synchronous generator and as a result the voltage and current at an IBR connected bus get modulated significantly. Thus there is a requirement to reassess the different protection principles employed for busbar.

Fault current contribution from an IBR may increase the current seen by the overcurrent relays protecting different lines in a distribution system, resulting in coordination problem and delayed decision [8, 9]. With significant phase and magnitude modulation of current, distance

Email address: soumitri.jena89@gmail.com (Soumitri Jena)

relays protecting lines connecting such renewable sources find problem with direction identification and reach during line fault [10, 11]. Current modulation from IBR decreases the operating current and may result in failure of the line differential relay [12].

The performance of transient based line differential protection connecting IBR proposed in [13] is constrained with the issues of synchronization error and dependency on communication infrastructure. Its performance is affected by over-damped transient present in fault current. Therefore transient based schemes cannot be used as standalone protection for transmission lines. Data mining and artificial intelligence techniques such as decision tree, fuzzy logic, neural networks, and related hybrid methods are proposed for IBR integrated transmission line protection [14, 15, 16]. Requirement of large scale training data addressing diversified control techniques limits its feasibility for practical applications.

Busbar protection is critical as it may be connected to several lines and generators in a substation. Directional protection schemes based on superimposed impedance [17, 18] provide better stability in current transformer (CT) saturation scenarios. Due to the requirement of voltage signals along with current signals, the cost and complexity increases in such schemes. In addition, the reliability of these schemes reduces in case multiple transmission lines connected to the busbar. The travelling wave based protection scheme presented in [19] provides high-speed protection for busbar faults. Performance of such a scheme jeopardizes for faults with small inception angle. Low-impedance percentage differential protection schemes [20, 21, 22] are most widely used for the protection of the busbar in a substation. Uncertain power system disturbances, close-in external faults and CT saturation may initiate false tripping of the above schemes. Such protection schemes may not detect internal busbar faults with high resistance due to insignificant operating current. The modulation in fault current magnitude and phase angle by the inverter may limit the performance of the differential relay when used for the bus connecting IBR to the grid. Large phase angle difference between both side currents results in malfunction of conventional current differential protection at times when the current magnitudes become comparable, such as faults involving significant resistance. The failure of substation busbar protection causes severe consequences like massive power outage, equipment damage and stability concern [23]. Therefore, in the presence of IBR there is a scope to develop reliable busbar protection methods.

In this work, the limitations of conventional differential protection for the busbar connecting a PV (photovoltaic) plant to the grid are demonstrated and a method using composite sequence currents is proposed. It uses positive sequence components for the differential current and negative and zero sequence components for the restraining current to derive the decision. As the negative sequence current is being suppressed by the control action of such inveter based resource and zero sequence current not available for ungrounded fault conditions, the use of positive sequence currents as differential current substantiates for all fault conditions. The restraining current is being emphasized to avoid maloperation due to CT saturation for external fault conditions. Use of negative and zero sequence components as restraining current prevents the unwanted maloperation due to CT saturation. The proposed method remains unaffected by the control action of the inverters, thereby mitigating the associated variation in fault characteristics. To evaluate the proposed method, the IEEE 9-bus system interconnecting a PV plant is used. The performance of the proposed method is demonstrated for different internal and external faults with change in PV plant capacity, fault condition and system parameters, with CT saturation, change in grid codes and found to be consistent. The comparative assessment with conventional differential protection depicts its superior performance.

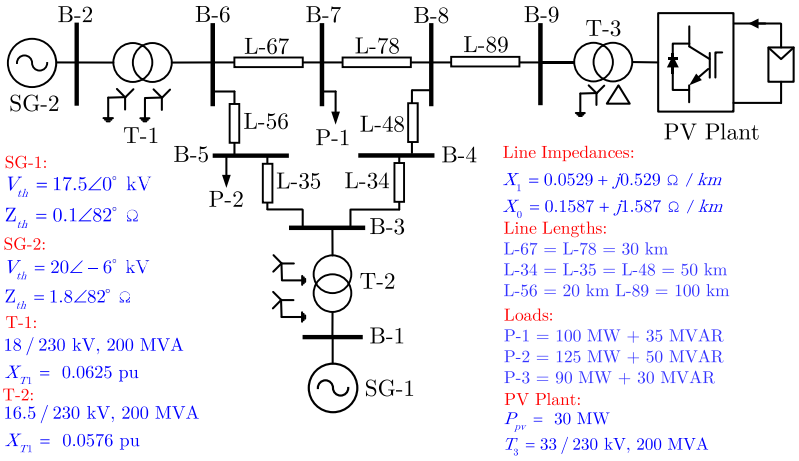

Figure 1: PV based IBR integrated IEEE 9-bus system.

2. System Description

The problem highlighted in this work and the evaluation of proposed method are carried out on IEEE 9-bus test system [24] integrating a PV plant, as shown in Fig. 1. Simulations are carried out in PSCAD/EMTDC software package [25]. The generator connected at bus-9 is replaced by a PV plant which comprises parallel combination of PV units to collectively generate a maximum of 30 MW power. Each PV unit consists of two parallel PV arrays followed by two-stage DC-DC and DC-AC conversion. A 33/230 kV step-up transformer is utilized to connect the grid. The phasor values used are estimated using one-cycle discrete Fourier transform with a signal sampling rate of 3.84 kHz.

The two-stage control scheme of the PV plant is depicted in Fig. 2. In the first stage, a DC booster has been used to maximize the power output from the PV (V_{pv}, I_{pv}) panels using MPPT control [26]. The second stage consists of a voltage source inverter (VSC) and its control scheme. The control strategy comprises of DC link voltage (V_{DC}) and reactive power (Q) balance controllers. The controllers work on a synchronous reference frame (dq) to regulate the fault current along the filter components (R_F, L_F, and C_F). Voltage and current disturbances from the grid side (V_{grid} and I_{grid}) are decoupled using proportional integral (PI) controllers, phase locked loop (PLL), and the dq components of voltage and current ($V_{d,q}$, and $I_{d,q}$). A pulse width modulator (PWM) and a comparator are used to trigger the VSC gate pulses. Step-up transformers (3/33 kV) are used to tap power from the PV units. Feed-forward positive sequence current compensation is provided for unrestrained controller operation for any disturbance in the grid side.

The FRT capability curve implemented in the PV plant inverter control is shown in Fig. 3. After inception of the fault, significant voltage drop may be experienced at the point of common coupling (PCC) of the PV plant. According to the FRT requirement, the PV plant remains connected to the power system for certain time if the voltage level is within the withstanding limit, otherwise it may be disconnected (as shown in the Fig.3). In such situations, the PV plant inverter supplies reactive current to increase the voltage level at PCC to an acceptable limit. The amount of reactive current injection depends on the applied grid code. The PV plant is complied with North American grid code (NA-GC) [27]. With such grid code compliance, the reactive

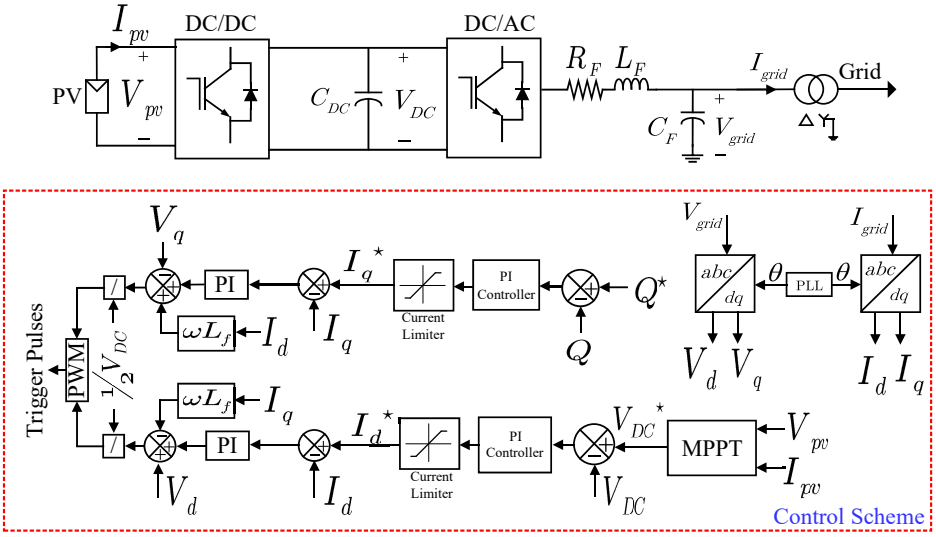

Figure 2: The control scheme applied to the PV Plant.

current injection is controlled to maintain a power factor between 0.95 lagging to 0.95 leading.

3. Problem Statement

3.1. Low-impedance Busbar Differential Protection

Low-impedance busbar differential protection, in both phasor and sampled value domain, provides high reliability and sensitivity. The phasor-based schemes usually adopt the relay characteristic as shown in Fig. 4. The tripping logic in phasor-based schemes compares the differential current I_{DIF} with the restraining current I_{RES} to detect any internal busbar fault.

$$I_{DIF} = \left| \sum_{p=1}^{P} I_p \right|; \qquad I_{RES} = \sum_{p=1}^{P} |I_p| \tag{1}$$

where, P is the total number of lines connected to the busbar and I_p is current flowing through the p-th line.

The relay decides based on,

$$I_{DIF} > I_{PU}; \quad AND \quad I_{DIF} > kI_{RES} \tag{2}$$

where the pick-up current (I_{PU}) is defined in terms of the maximum feeder current multiplied by a safety factor. CT saturation is the main concern while considering the reliability of the busbar differential relay. Two different operational slopes (k_1 and k_2) are used for the trip decision. Following detection of an external fault, the relay enters to a high-security mode, during which it dynamically selects the higher slope. The configured relay settings in this work which are in accordance with available relays [28] are presented in Table 1.

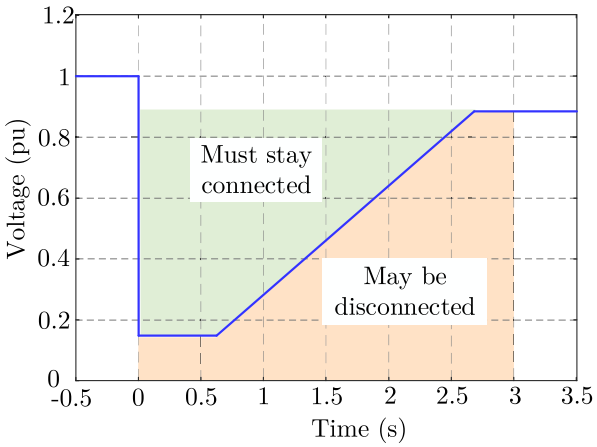

Figure 3: FRT capability curve in the proposed method.

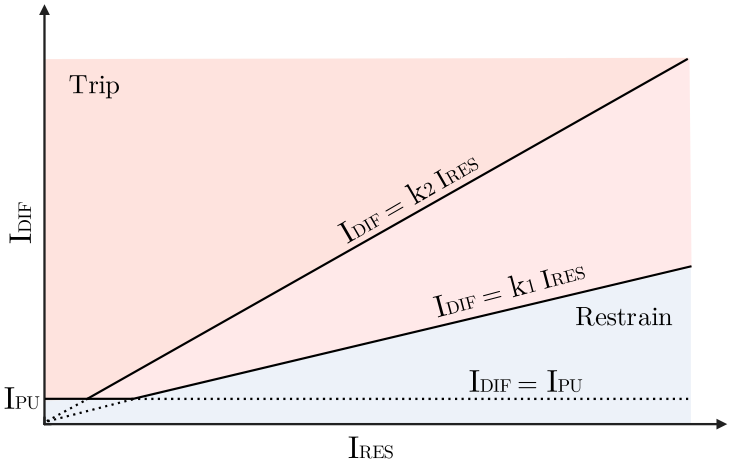

Figure 4: Low-impedance busbar differential relay characteristics.

Table 1: Relay settings for the proposed work

Relay Element	Settings	
	Range	Selected
Pick-up Current (I_{PU})	0.1-4 pu	0.2 pu
Slope-1 (k_1)	15-90%	25%
Slope-2 (k_2)	50-90%	75%

3.2. Conventional Protection with IBR Integration

Fig. 5 shows the PV plant connected to the bus-9(M) of the test system through a 33/230 kV step-up transformer. I_M and I_N represent the acquired current from the PV and the grid side for the protection of bus-9(M). Z_L denotes the impedance of the transmission line connecting bus-9 (M) and bus-8 (N). The equivalent voltage and impedance of the rest of synchronous grid are represented using E_N and Z_N, respectively.

The magnitude and phase angle of fault current in IBRs are significantly different from the conventional synchronous sources. It adversely affect the low-impedance busbar differential protection designed for synchronous grid environments. The fault current contribution from the PV power plant is limited due to the inverter limiter set to the values close to nominal fault current. Moreover, the fault response from the IBR depends, to a large extent, on the control strategy. The phase angle fault current from the inverter depends on the control action. With the inverter control action, current magnitude from the IBR side is limited. In general, both side current magnitudes for an internal fault is related as,

$$\left|\dot{I}_N\right| = h\left|\dot{I}_M\right| \tag{3}$$

where h is a multiplying factor and greater than 1. The notation [˙] stands for the phasor values. The differential and restraining currents are obtained as,

$$\begin{aligned} I_{DIF} &= \left|\dot{I}_M + \dot{I}_N\right| = |I_M\angle\theta_M + hI_M\angle\theta_N| \\ &= I_M\sqrt{\left|1 + h^2 + 2h\cos\left(\theta_M - \theta_N\right)\right|} \end{aligned} \tag{4}$$

$$I_{RES} = \left|\dot{I}_M\right| + \left|\dot{I}_N\right| = I_M + hI_M = I_M\left(1 + h\right) \tag{5}$$

where θ_m and θ_n are current phase angles of IBR and grid side, respectively. As seen in (4) and (5), in addition to the fault current magnitude from both the sides, the differential current depends on the cosine of phase angle difference between current phasors, whereas the restraining current is independent of phase angles. The operational slope k is obtained from (4) and (5) as,

$$k = \frac{\sqrt{[1 + h^2 + 2h\cos(\theta_M - \theta_N)]}}{1 + h} \tag{6}$$

It is noteworthy to point out from (6) that h, θ_M, and θ_N are the decisive factors for the differential protection operation.

3.3. Simulation Studies

The performance of conventional current differential relay is tested on the system of Fig. 5 for different internal faults with variation in IBR and grid parameters. The steady-state operating points are shown in Fig. 6 with the relay settings as per Table 1. Fault resistance, length of grid connecting line and grid equivalent impedance are varied at a time for different PV plant output level, by keeping other parameters as fixed. The observations from the obtained results are as follows:

1. Fault current from IBR increases with higher integration level. This reduces the magnitude difference between both end currents. Large angle difference between the currents in such a situation reduces the differential current significantly and leads the relay to malfunction.

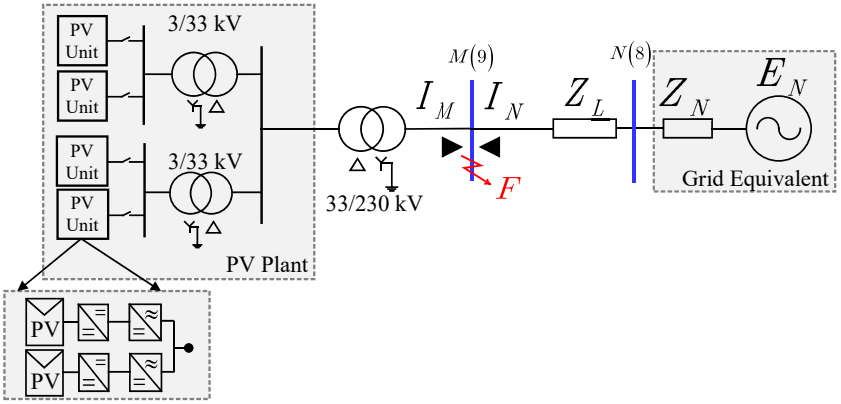

Figure 5: PV based IBR connected to the grid equivalent circuit.

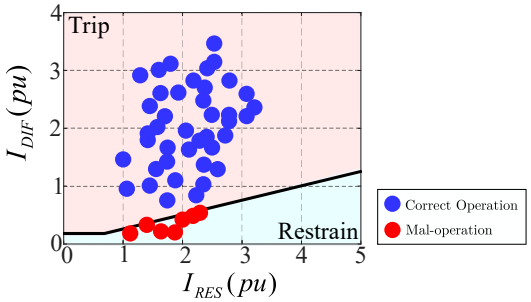

PV integration / Parameters	$L = 25\ km$, $Z_N = 1\ pu$				$R_f = 40\ \Omega$, $Z_N = 1\ pu$				$L = 25\ km$, $R_f = 40\ \Omega$			
	Fault Resistance: $R_f(\Omega)$				Line Length: L (km)				Grid Equivalent Impedance: $Z_N(pu)$			
P_{pv}	20	40	60	80	25	50	75	100	0.8	1.0	1.2	1.4
7.5 MW	●	●	●	●	●	●	●	●	●	●	●	●
15 MW	●	●	●	●	●	●	●	●	●	●	●	●
22.5 MW	●	●	●	●	●	●	●	●	●	●	●	●
30 MW	●	●	●	●	●	●	●	●	●	●	●	●

Figure 6: Response of conventional busbar differential protection scheme with variations system and grid parameters

2. IBR current being limited, R_f mainly affects the grid side current magnitude. Thus with increase in R_f, magnitude difference between both side currents reduces and makes the relay vulnerable to malfunction.
3. Similar to R_f, the increase in line length and equivalent grid impedance also reduces the grid side current contribution for internal faults. Thus the differential relay protecting a busbar with such a connectivity is prone to malfunction for long lines and weak grid conditions.

Thus there is a need of an alternative technique to prevent such relay maloperations which should be independent of system and fault parameter variations.

4. Proposed Method

In this section, a protection method is proposed, where the differential and restraining currents are derived using sequence current components. Negative sequence current from the IBR may be negligible even for asymmetrical faults. On the other hand, zero sequence current is not available in case of ungrounded faults. Thus, the positive sequence current is only found to be suitable for using as differential current with such connectivity. Limitation of fault current from IBR eliminates the possibility of CT saturation for grid side external faults. In case of a fault on the IBR side, there is a possibility of CT saturation as the current in both side CTs are fed by the grid. Due to increase in phase current asymmetry during CT saturation (even for balanced faults), negative and zero sequence currents become prominent [29]. Thus the use of negative and zero sequence components as restraining current can provide better security for the busbar protection. Exploring the advantages of these composite sequence currents (*i.e.* availability of positive sequence current for all types of faults and improved security provided by negative and zero sequence currents), the differential and restraining currents are obtained by analysing the sequence networks for different fault types as shown in Fig. 7. The notations used in Fig. 7 are given in Table. 2.

4.1. Internal Faults

4.1.1. AG Fault

For a phase-A-ground (AG) fault on the busbar, the corresponding sequence network is shown in Fig. 7 (a). As the negative sequence current contributed by the IBR is negligible during the fault, corresponding path is considered as an open circuit in the sequence network.With such a network, the relation between the sequence current can be expressed as,

$$\dot{I}_{M1} + \dot{I}_{N1} = \dot{I}_{M2} + \dot{I}_{N2} = \dot{I}_{M0} + \dot{I}_{N0} \tag{7}$$

where $\dot{I}_M$, and $\dot{I}_N$ are the IBR and grid side currents, respectively, and $\dot{I}_{M2} = 0$. Subscripts 1, 2 and 0 represent the positive, negative and zero sequence components, respectively.

The relationship in (7) can be rewritten as,

$$\left|\dot{I}_{M1} + \dot{I}_{N1}\right| = 0.5\left(\left|\dot{I}_{M2} + \dot{I}_{N2}\right| + \left|\dot{I}_{M0} + \dot{I}_{N0}\right|\right) \tag{8}$$

Considering the left side of (8) having positive sequence currents as the I_{DIF} and right side consisting of negative and zero sequence current as the I_{RES}, the trajectory of relay operating point for AG fault can be found on the blue dotted line in Fig. 8. The trajectory position above

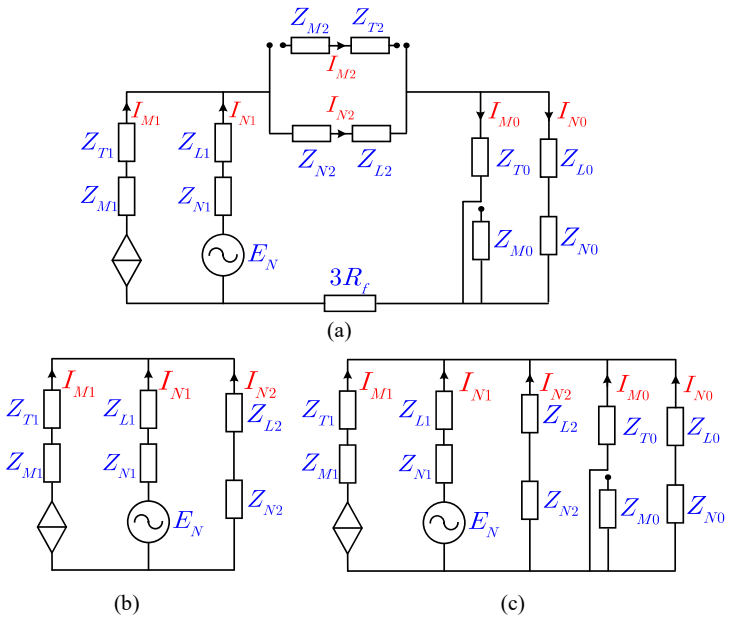

Figure 7: Sequence networks for (a) AG (b) BC and (c) BCG faults on the system.

Table 2: Notations used for the sequence network analysis.

Notation	Explanation
Z_{M1}	Positive sequence impedance of the IBR
Z_{T1}	Positive sequence impedance of the transformer connecting IBR
Z_{T1}	Positive sequence current from the IBR
E_N	Equivalent grid voltage
Z_{N1}	Positive sequence impedance of the grid
Z_{L1}	Positive sequence impedance of the transmission line MN
I_{N1}	Positive sequence current from the grid
Z_{M2}	Negative sequence impedance of the IBR
Z_{T2}	Negative sequence impedance of the transformer connecting IBR
I_{M2}	Negative sequence current from the IBR
Z_{N2}	Negative sequence impedance of the grid
Z_{L2}	Negative sequence impedance of the transmission line MN
I_{N2}	Negative sequence current from the grid
Z_{M0}	Zero sequence impedance of the IBR
Z_{T0}	Zero sequence impedance of the transformer connecting IBR
I_{M0}	Zero sequence current from the IBR
Z_{N0}	Zero sequence impedance of the grid
Z_{L0}	Zero sequence impedance of the transmission line MN
I_{N0}	Negative sequence current from the grid
R_f	Fault resistance

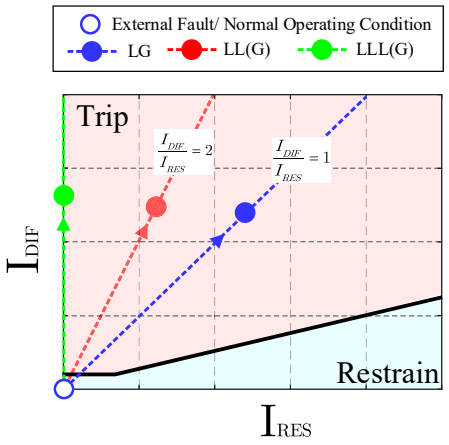

Figure 8: Fault characteristics in the proposed method.

the set differential characteristic (with $k = 0.25$), as shown in Fig. 8, ensures correct detection of such a fault type. Such a selection of differential and restraining currents provides sufficient security in the protection scheme and even for other types of faults analyzed below.

4.1.2. BC Fault

Fig. 7 (b) represents the sequence network for BC fault. The relation between sequence currents can be expressed as,

$$\dot{I}_{M1} + \dot{I}_{N1} = -\dot{I}_{N2} \tag{9}$$

Above relation can be rewritten as,

$$\left|\dot{I}_{M1} + \dot{I}_{N1}\right| = 2\left[0.5\left(\left|\dot{I}_{M2} + \dot{I}_{N2}\right| + \left|\dot{I}_{M0} + \dot{I}_{N0}\right|\right)\right] \tag{10}$$

No zero sequence current is present for such an ungrounded fault and the solar plant does not generate negative sequence current. Thus, $\dot{I}_{M2} = \dot{I}_{M0} = \dot{I}_{No} = 0$ in (10).

According to (10), the relay operating point follows the trajectory on red dotted line in Fig. 8, when I_{DIF} and I_{RES} are used similar as used for AG fault and confirms its detection.

4.1.3. BCG fault

With the sequence network of Fig. 7 (c), the relation between sequence current for BCG fault can be expressed as,

$$\dot{I}_{M1} + \dot{I}_{N1} = -\left(\dot{I}_{N2} + \dot{I}_{M0} + \dot{I}_{N0}\right) \tag{11}$$

dYg type connection of IBR connecting transformer helps to maintain homogeneity in the zero sequence network. Phase angle difference of negative and zero sequence impedances being very small for a conventional transmission network [30], $\dot{I}_{N2}$ and $\dot{I}_{N0}$ remain in phase with each other for BCG fault. Considering this equal phase relationship of $\dot{I}_{N2}$, $\dot{I}_{M0}$, and $\dot{I}_{N0}$, (11) can be rewritten as,

$$\left|\dot{I}_{M1} + \dot{I}_{N1}\right| = \left|\dot{I}_{N2} + \dot{I}_{M0} + \dot{I}_{N0}\right| = \left|\dot{I}_{N2}\right| + \left|\dot{I}_{M0} + \dot{I}_{N0}\right| \tag{12}$$

By introducing $\dot{I}_{M2}$ in (12), the relation can be expressed as,

$$\left|\dot{I}_{M1} + \dot{I}_{N1}\right| = 2\left[0.5\left(\left|\dot{I}_{M2} + \dot{I}_{N2}\right| + \left|\dot{I}_{M0} + \dot{I}_{N0}\right|\right)\right] \tag{13}$$

Thus, the trajectory of relay operating point follows the same red dotted line in Fig. 8 for BCG fault also and detects the fault correctly.

4.1.4. Symmetrical fault

In case of balanced fault (LLL(G)), restrain current become zero due to the absence of negative and zero sequence currents. Thus the operating point follows the green dotted line (Fig. 8) through vertical axis and performs correctly.

4.2. External Fault and Normal Operating Condition

For external faults on either side of the busbar, the sequence currents become equal in amplitude but opposite in direction. Thus the phasor sum of individual sequence components become zero and the relay maintains sufficient security for such a situation as shown in Fig. 8. The same argument is also valid for normal operating conditions.

4.3. Overall Description of the Proposed Method

The flow diagram shown in Fig. 9 summarises the overall process of the proposed method. The phasor computation is carried out with full-cycle discrete Fourier transform with anti-aliasing filter to obtain the sequence components. Based on the sequence network analysis presented above, the differential and restraining currents are established. The differential current is compared with the pick-up current (I_{PU}) and k times the restraining current to identify the internal fault.

5. Results and Discussion

The proposed protection method is evaluated and compared with the conventional low-impedance busbar differential protection using fault signals simulated on the test system. An extensive range of simulations is carried out by changing the system and fault parameters. Comparative assessment reveals that proposed method performs correctly when conventional protection scheme maloperates.

5.1. Performance for Different Fault Types

5.1.1. Ground Faults

A line-to-ground fault in phase-A (AG) with fault resistance 50 Ω is created on the busbar. Figs. 10 (a)-(b) show the current waveforms of M and N sides, respectively. It can be noticed that the the current phase angles of each phase PV current is roughly same therefore the contribution of zero sequence current is significant. Apart from the zero-sequence current, only positive sequence current contributes to the fault current as of the negative sequence current contribution from the IBR is negligibly small. The current phase angle differences ($\theta_m - \theta_n$) are shown in Fig. 10 (c). The responses of the conventional scheme and the proposed method are shown in Fig. 11 (a) and (b), respectively. The operating point in the proposed method moves into the trip region after occurrence of the fault whereas the conventional scheme fails to operate.

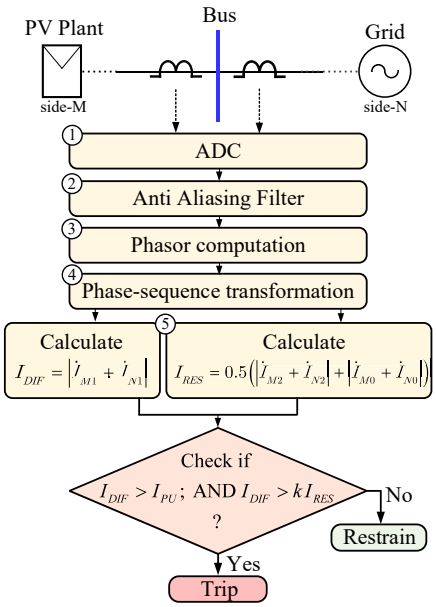

Figure 9: Flow diagram of the proposed scheme.

5.1.2. Ungrounded faults

A line-to-line fault (AB) is simulated on the busbar. The fault current waveforms of the PV plant and the grid are shown in Fig. 12 (a) and (b), respectively. The fault current waveforms of the PV plant are almost symmetrical. The fault current waveforms from the grid differ from the PV plant, where both positive and negative sequence fault currents are of equal prominence. The current phase angle differences of both phase-A and B are shown in Fig. 12 (c). It can be observed that the angle difference for phase-B is higher when compared to phase-A. The responses of the conventional scheme and proposed method are depicted in Fig. 13 (a) and (b), respectively. The phase-B relay element under this condition does not operate while phase-A element is on the edge of operation. Upon a closer observation, it can be verified that the proposed method with sequence components clearly identifies the fault. The results are in similar terms with the theoretical analysis presented in the previous section and validates the proposed method.

5.2. Performance for Different Fault Resistances

Aiming to evaluate performance of the proposed method for different fault resistances, line-to-ground faults (CG type) with fault resistance 25-100 Ω are simulated on the busbar. The comparative analysis of the conventional protection and proposed method is presented in Fig. 14 (a) and (b), respectively. As depicted in Fig. 14, the conventional protection fails for higher fault resistance. The proposed method has been consistent in detecting all the fault cases presented here as operating point remains inside the trip region.

5.3. Performance with Change in Grid Equivalent Impedance

To test the effectiveness of the proposed method for variations in system parameters, Z_N is varied. Under these conditions, BCG faults are simulated on the busbar. The steady state

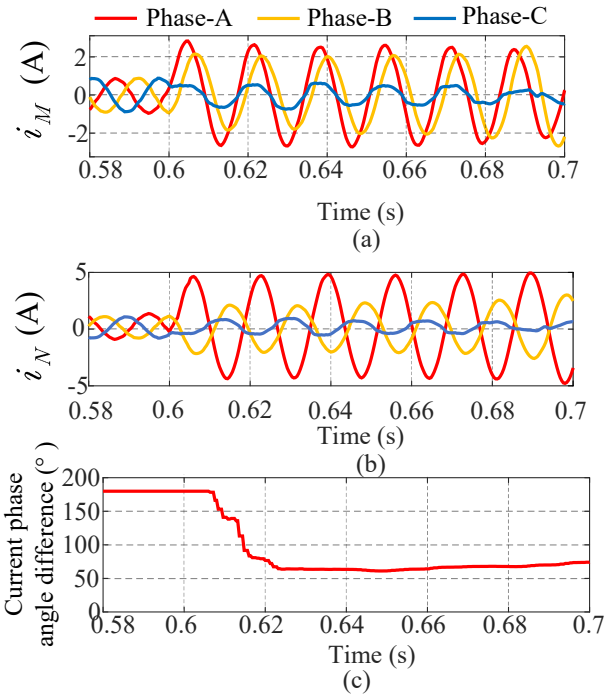

Figure 10: Current waveforms from (a) PV plant and (b) grid for AG fault on the busbar; (c) phase angle difference of both side currents.

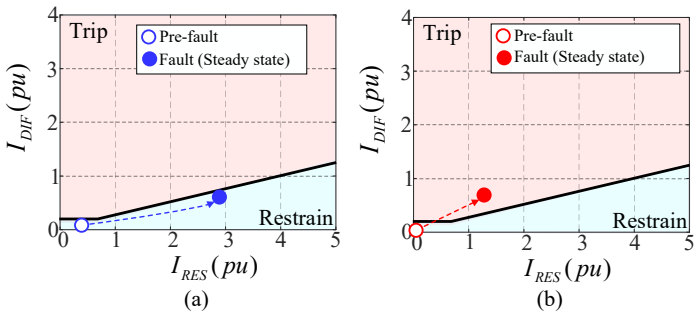

Figure 11: Response of (a) conventional scheme and (b) proposed method for LG fault.

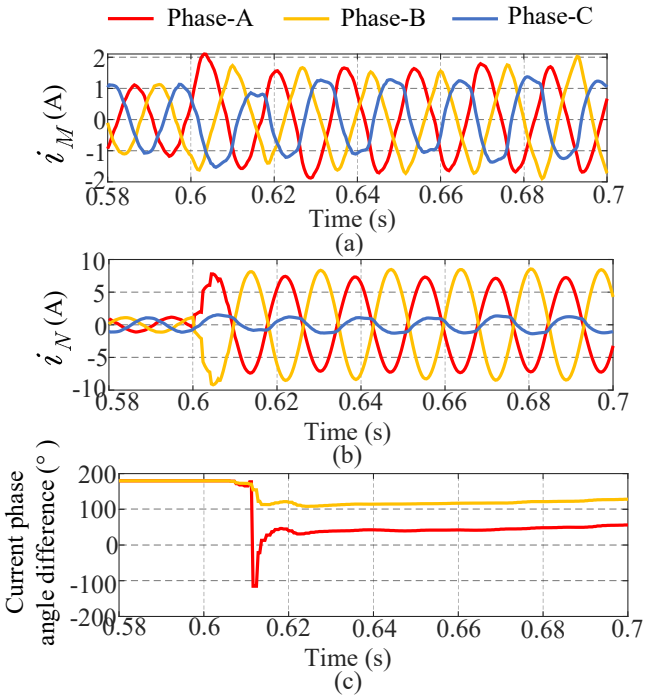

Figure 12: Current waveforms from (a) PV plant and (b) grid for AB fault on the busbar; (c) phase angle difference of both side currents.

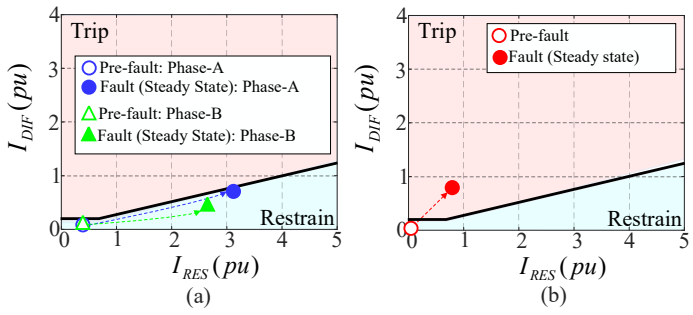

Figure 13: Response of (a) conventional scheme and (b) proposed method for LL fault.

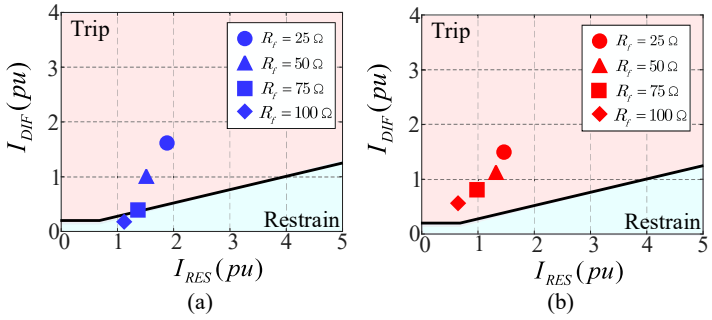

Figure 14: Performance of (a) conventional scheme (b) proposed method during internal faults with different fault resistances.

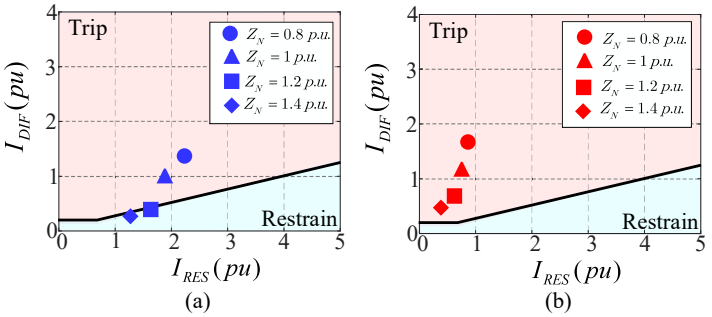

Figure 15: Performance of (a) conventional scheme (b) proposed method during internal faults with different grid equivalent impedance

operating points in such fault scenarios for the conventional scheme and proposed method are presented in Fig. 15 (a) and (b). It is observed from Fig. 15 (a) that the conventional scheme fails to to operate for higher grid impedance values (weaker grids). Performance of the proposed method, as seen in Fig. 15 (b), remains consistent in correctly identifying the internal faults even with the change in grid parameters.

5.4. Performance for Different Levels of PV Integration

As discussed previously, the relative strength between the IBR and the grid is vital for differential protection performance. If the difference between fault current amplitude of the PV plant and the grid side is large then the differential current will be sufficient. However, if current from both the sources are relatively comparable then the differential current may not be sufficient for an internal busbar fault. To verify this, A-G faults are simulated on the busbar with different levels of PV integration. The results obtained as the steady state operating point for the conventional scheme and proposed method are shown in Fig. 16 (a) and (b), respectively. As observed in Fig. 16 (a), the operating point for higher values of PV integration remains inside the restraining region leading to the failure of the conventional protection. On the contrary, the proposed method correctly detects busbar faults even with higher levels of PV integration.

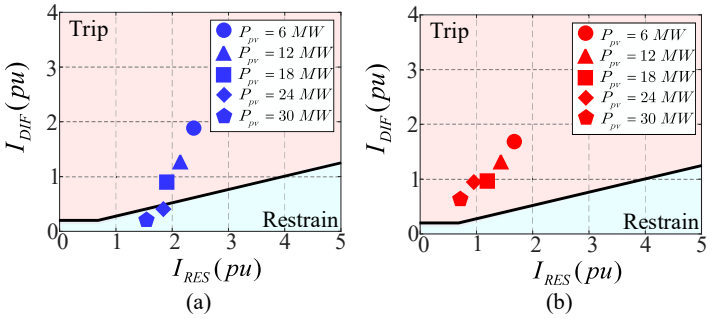

Figure 16: Performance of (a) conventional scheme (b) proposed method during internal faults with change in PV integration.

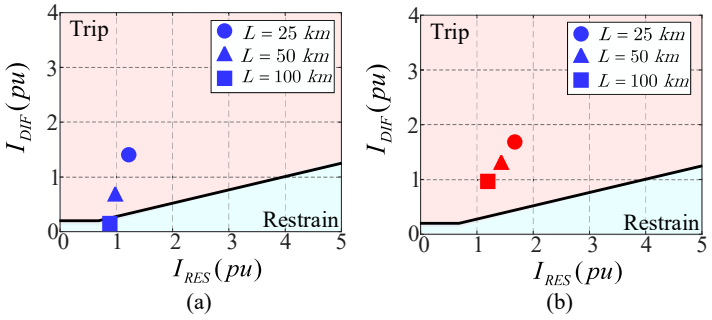

Figure 17: Performance of (a) conventional scheme (b) proposed method during internal faults with change in line length.

5.5. Performance with Change in Line Length

To verify the performance of proposed method for different lengths of transmission lines, A-G faults are simulated on the busbar. The length of the transmission line (L) is varied between 50~100 km. The performance of conventional scheme and proposed method in such cases are shown in Fig. 17 (a) and (b), respectively. It is observed from Fig. 17 (a) that the conventional protection is at higher risk for longer transmission lines. On the contrary, it is evident in Fig. 17 (b) that the proposed method has been able to detect all the aforementioned faults. Conclusively, the proposed method is more efficient in detecting faults with longer transmission lines connected.

5.6. External Faults with or without CT saturation

To verify the stability of the proposed method for external fault and CT saturation conditions, symmetrical faults (ABC) are simulated on the IBR side. Fig. 18 (a) shows the response of the proposed method for an external fault on the PV side at a distance of 10 km from the busbar. All the sequence components in this condition are of equal magnitude and opposite direction which results in zero differential and restraining currents. Therefore, it is to be observed from Fig. 18 that the operating point lies close to the origin. Thus, stability against external faults can be assured by the proposed method. As discussed previously, an external fault on the grid side does not draw very high fault current because of the inverter current limitation. Therefore, the

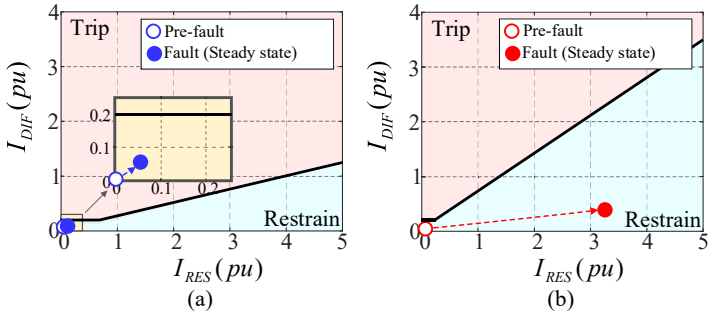

Figure 18: Response of proposed method for (a) external fault and (b) CT saturation.

probability of CT saturation can be avoided. On the contrary, a fault on the PV side may draw high current to saturate one of the CTs. In this regard, a fault of ABC type on the PV side is simulated at a distance of 1 km from the busbar. In order to have the CT saturation condition, the burden resistance is increased 10 times of its nominal value. Fig. 18 (b) shows the response of the proposed method for this condition. The saturated CT waveforms predominately consist of zero and negative sequence components of current. Therefore, The operating point is observed to be shifting towards right because of the higher restraining current. In such a condition, the relay dynamically selects the higher slope (slope 2) to gain higher security against CT saturation [28]. As evident from the analysis and the obtained results, restraining current defined in terms negative and zero sequence currents provides stability for CT saturation condition.

5.7. Performance with Change in Grid Code Requirement

In order to verify the performance of the proposed method with change in grid code requirements, the European Union grid code (EU-GC) [31] is complied with the IBR. NA-GC does not enforce any specific regulation on the active or reactive components of fault current to ride through the fault. With continuous advancement in grid codes, available solar plants are found with different control strategies. In contrast, the EU-GC necessitates reactive power support in case of fault conditions. The new EN 50549 [32, 33] series of standards are very close in definition with [31]. The major difference in FRT requirements are for the recovery of the voltage after the clearance of the fault, where the requirements vary from 1.5 to 3.0 s. The fault current injection capabilities vary for different countries. In order to test the adaptability of proposed method for different grid codes, solid AG faults are simulated on the test system with both NA-GC and EU-GC compliances separately. Figs. 19 (a) and (b) show the results obtained for the two fault cases with NAGC and EU-GC, respectively. The relay trajectory in both the cases move into the trip region following the fault inception. Thus the proposed sequence component based method performs correctly for busbar protection irrespective of the control strategy applied to the IBR. The proposed method being developed based on the sequence current angle properties in the faulted path, it is independent of inverter control schemes. The equations used for different fault types in the proposed method utilize negative sequence current measurement from the PV side. Therefore, the proposed method can perform correctly even with the grid codes which mandate the inverter to supply negative sequence current.

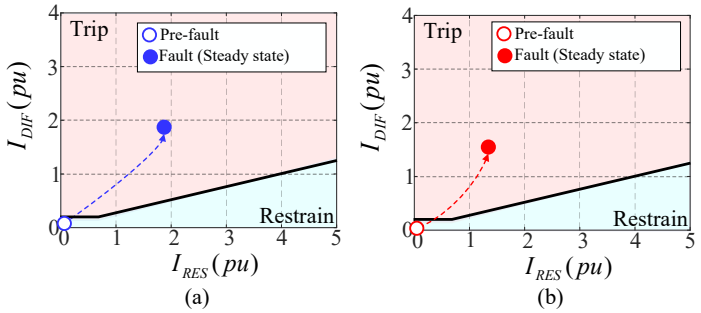

Figure 19: Performance of proposed scheme for (a) NA-GC, (b) EU-GC during AG fault.

6. Conclusion

The challenges in differential protection of the busbar connecting IBRs to the the grid are of significance. The large phase angle differences between both end currents for certain fault conditions may lead to malfunction of the available busbar protection. To this end, the work proposes a differential protection approach based on the composite sequence currents. The differential current for the proposed method is obtained from the positive sequence components from both IBR and grid side currents. The negative and zero sequence currents are utilized to provide effective restrain to external faults. The influencing factors for the relay failure are studied, and the performance of proposed method for these conditions has been analysed. Proposed method remains immune to the inverter control action and associated variations in fault characteristics. Theoretical and simulation studies conclude that the proposed method provides better performance resulting reliable and secure operation compared to the conventional low-impedance differential protection. Its performance remains consistent for the change in fault type, fault resistance, transmission line length, system parameters, PV integration level, and grid code. Performance of the proposed method for external fault and CT saturation conditions demonstrates its robustness in preventing mal-operation. The proposed method exhibits better performance particularly with large scale integration of IBRs which will be crucial in future grids.

References

[1] Government of India: Ministry of New and Renewable Energy, Guidelines for Implementation of Scheme for Setting up of 750 MW Grid-connected Solar PV Power Projects under Batch-1 (October, 2013).
URL `https://www.seci.co.in/web-data/docs/final-VGF_750MW_Guidelines_for-grid-solar-power-projects.pdf`

[2] R. Kabiri, D. G. Holmes, B. P. McGrath, Control of active and reactive power ripple to mitigate unbalanced grid voltages, IEEE Transactions on Industry Applications 52 (2) (2015) 1660–1668.

[3] Z. Shuai, C. Shen, X. Yin, X. Liu, Z. J. Shen, Fault analysis of inverter-interfaced distributed generators with different control schemes, IEEE Transactions on Power Delivery 33 (3) (2018) 1223–1235.

[4] F. Blaabjerg, R. Teodorescu, M. Liserre, A. V. Timbus, Overview of control and grid synchronization for distributed power generation systems, IEEE Transactions on industrial electronics 53 (5) (2006) 1398–1409.

[5] A. Camacho, M. Castilla, J. Miret, J. C. Vasquez, E. Alarcón-Gallo, Flexible voltage support control for three-phase distributed generation inverters under grid fault, IEEE transactions on industrial electronics 60 (4) (2012) 1429–1441.

[6] H. M. Hasanien, An adaptive control strategy for low voltage ride through capability enhancement of grid-connected photovoltaic power plants, IEEE Transactions on Power Systems 31 (4) (2016) 3230–3237.

[7] Y. Wang, B. Ren, Fault ride-through enhancement for grid-tied pv systems with robust control, IEEE Transactions on Industrial Electronics 65 (3) (2018) 2302–2312.
[8] Y. Firouz, S. Farhadkhani, J. Lobry, F. Vallée, A. Khakpour, O. Durieux, Numerical comparison of the effects of different types of distributed generation units on overcurrent protection systems in mv distribution grids, Renewable Energy 69 (2014) 271–283.
[9] L.-H. Chen, Overcurrent protection for distribution feeders with renewable generation, International Journal of Electrical Power & Energy Systems 84 (2017) 202–213.
[10] A. Hooshyar, M. A. Azzouz, E. F. El-Saadany, Distance Protection of Lines Emanating From Full-Scale Converter-Interfaced Renewable Energy Power Plants—Part I: Problem Statement, IEEE Transactions on Power Delivery 30 (4) (2015) 1770–1780.
[11] S. Paladhi, A. K. Pradhan, Adaptive distance protection for lines connecting converter-interfaced renewable plants, IEEE Journal of Emerging and Selected Topics in Power Electronics (Early Access) (2020).
[12] K. Jia, Y. Li, Y. Fang, L. Zheng, T. Bi, Q. Yang, Transient current similarity based protection for wind farm transmission lines, Applied Energy 225 (2018) 42–51.
[13] S. Kar, S. R. Samantaray, Time-frequency transform-based differential scheme for microgrid protection, IET Generation, Transmission & Distribution 8 (2) (2014) 310–320.
[14] M. K. Jena, S. R. Samantaray, Data mining based intelligent differential relaying for transmission lines including UPFC and wind farms, IEEE Transactions on Neural Networks and Learning Systems 27 (1) (2016) 8–17.
[15] M. K. Jena, S. R. Samantaray, L. Tripathy, Decision tree-induced fuzzy rule-based differential relaying for transmission line including unified power flow controller and wind-farms, IET Generation, Transmission Distribution 8 (12) (2014) 2144–2152.
[16] D. P. Mishra, S. R. Samantaray, G. Joos, A combined wavelet and data-mining based intelligent protection scheme for microgrid, IEEE Transactions on Smart Grid 7 (5) (2016) 2295–2304.
[17] M. Eissa, A novel digital directional technique for bus-bars protection, IEEE Transactions on Power Delivery 19 (4) (2004) 1636–1641. doi:10.1109/TPWRD.2004.835271.
[18] M. R. D. Zadeh, T. S. Sidhu, A. Klimek, Implementation and testing of directional comparison bus protection based on iec61850 process bus, IEEE Transactions on Power Delivery 26 (3) (2011) 1530–1537. doi:10.1109/TPWRD.2010.2060213.
[19] G. Zou, H. Gao, A traveling-wave-based amplitude integral busbar protection technique, IEEE Transactions on Power Delivery 27 (2) (2012) 602–609. doi:10.1109/TPWRD.2012.2184561.
[20] Y.-C. Kang, U.-J. Lim, S.-H. Kang, P. Crossley, A busbar differential protection relay suitable for use with measurement type current transformers, IEEE Transactions on Power Delivery 20 (2) (2005) 1291–1298. doi:10.1109/TPWRD.2004.834325.
[21] A. Guzman, B.-L. Qin, C. Labuschagne, Reliable busbar protection with advanced zone selection, IEEE Transactions on Power Delivery 20 (2) (2005) 625–629. doi:10.1109/TPWRD.2004.834671.
[22] N. Villamagna, P. Crossley, A ct saturation detection algorithm using symmetrical components for current differential protection, IEEE Transactions on Power Delivery 21 (1) (2006) 38–45. doi:10.1109/TPWRD.2005.848654.
[23] Exploring the IEEE C37.234 guide for protective relay application to power system buses, IEEE Transactions on Power Delivery 26 (2) (2011) 936–943. doi:10.1109/CPRE.2011.6035602.
[24] A. Banaiemoqadam, A. Hooshyar, M. A. Azzouz, A control-based solution for distance protection of lines connected to converter-interfaced sources during asymmetrical faults, IEEE Transactions on Power Delivery 35 (3) (2020) 1455–1466. doi:10.1109/TPWRD.2019.2946757.
[25] Manitoba HVDC Research Centre,, PSCAD ver. 4.6, EMTD (Software Package), Winnipeg, MB, Canada.
[26] M. A. G. De Brito, L. Galotto, L. P. Sampaio, G. d. A. e Melo, C. A. Canesin, Evaluation of the main mppt techniques for photovoltaic applications, IEEE transactions on industrial electronics 60 (3) (2012) 1156–1167.
[27] North American Electric Reliability Corporation, Reliability Guideline: Improvements to Interconnection Requirements for BPS-Connected Inverter-Based Resources, September 2019.
URL https://www.nerc.com/comm/PC_Reliability_Guidelines_DL/Reliability_Guideline_IBR_Interconnection_Requirements_Improvements.pdf
[28] Schweitzer Engineering Laboratories, SEL-487B-1 Bus Differential Relay, Sel-487b-1 bus differential relay, Pullman, WA-USA.
URL https://cms-cdn.selinc.com/assets/Literature/Product%20Literature/Data%20Sheets/487B-1_DS_20200229.pdf?v=20200417-200934
[29] N. Villamagna, P. A. Crossley, A ct saturation detection algorithm using symmetrical components for current differential protection, IEEE Transactions on Power Delivery 21 (1) (2006) 38–45. doi:10.1109/TPWRD.2005.848654.
[30] G. Ziegler, Numerical Differential Protection: Principles and Applications, John Wiley & Sons, USA, 2012.
[31] European Grid Code, Ordinance on system services by wind energy plants (System service ordinance—SDLWindV), Jun 2010.

URL www.erneuerbare-energien.de/fileadmin/ee-import/files/english/pdf/application/pdf/sdl_windv_en.pdf

[32] EN 50549-1:2019: Requirements for generating plants to be connected in parallel with distribution networks - Part 1: Connection to a LV distribution network - Generating plants up to and including Type B, European Committee for Electrotechnical Standardization (2019).

[33] EN 50549-2:2019: Requirements for generating plants to be connected in parallel with distribution networks - Part 2: Connection to a MV distribution network - Generating plants up to and including Type B, European Committee for Electrotechnical Standardization (2019).